ACS OMEGA

Open Access

http://pubs.acs.org/journal/acsodf

Article

Multifunctional Chitosan Nanofiber-Based Sponge Materials Using Freeze−Thaw and Post-Cross-Linking Method

Madhurangika Panchabashini Horathal Pedige, Akihide Sugawara,* and Hiroshi Uyama*

Cite This: *ACS Omega* 2024, 9, 36464−36474

Read Online

ACCESS | Metrics & More | Article Recommendations | Supporting Information

ABSTRACT: The fabrication of porous sponge materials with stable structures via cross-linking diverse polymers presents significant challenges due to the simultaneous requirements for phase separation as a pore-forming step and cross-linking reactions during the fabrication process. To address these challenges, we developed a sponge material solely from natural-based polymers, specifically chitosan nanofibers (CSNFs) and dialdehyde carboxymethyl cellulose (DACMC), employing a straightforward, eco-friendly technique. This technique integrates a facile freeze−thaw method with subsequent cross-linking between CSNFs and DACMC. This method effectively addresses the difficulties associated with pore formation in materials, which typically arise from the rapid formation and precipitation of polyionic complexes during the mixing of anionic and cationic polymers, using ice crystals as a rigid template. The resultant sponge materials exhibit remarkable shape recoverability in their wet state and maintain light, stable porosity in the dry state. Furthermore, in comparison to commonly used commercial foams, this composite porous material demonstrates superior fire retardancy and thermal insulation properties in its dry state. Additionally, it shows effective adsorption capacities for both cationic and anionic dyes and metal ions. This method of using biobased polymers to produce porous composites offers a promising avenue for creating multifunctional materials, with potential applications across various industries.

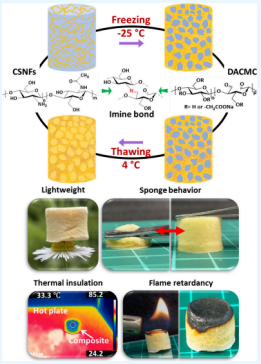

INTRODUCTION

Sponges are defined as fibrous porous materials featuring three-dimensional (3D) networks that display reversible compressibility, mechanical integrity, and low bulk density. These materials are characterized by their breathability, low bulk density, and substantial pore volume, enabling the integration of various functional properties, thus enhancing their versatility for multiple applications.[1] The synthesis of sponge materials commonly employs techniques such as electrospinning, particulate leaching, freeze-casting, and thermally induced phase separation.[2] The prevalent template growth method uses sacrificial materials to create pores, however, this approach often confronts challenges in eliminating residual templates and unreacted chemicals.[3−6] Ice crystals are advantageous as porogens, simplifying the template removal process through the freezing of aqueous media and subsequent removal of water by drying, solvent exchange, or lyophilization.[7] The freeze−thaw method stands out as a particularly effective technique for synthesizing porous 3D networks utilizing, ice crystals as porogens. This method promotes the formation of physical entanglements among polymers by concentrating them through the segregation and confinement within frozen solvent crystals.[8] However, the development of porous structures with adequate mechanical durability is contingent upon the choice of polymers, which must be capable of forming robust interactions among themselves. Consequently, the range of polymers suitable for creating porous sponges through simple freeze−thaw cycles is limited. Therefore, there is a critical need to develop versatile methodologies for fabricating sponge materials that extend the range of applicable polymers through the use of eco-friendly freeze−thaw processes. The introduction of cross-linking within a polymer network is a widespread and efficacious strategy to enhance the mechanical and structural stability of porous materials.[9] However, forming cross-links under freezing conditions presents difficulties, as the diffusion of chemicals is significantly reduced and reactivity is diminished in cold and frozen media. Moreover, a complex technique is necessary to manage the simultaneous occurrence of phase separation during the pore-forming step and the cross-linking reaction in the fabrication process. Accordingly, this study emphasizes the strategic use of thawing steps, typically overlooked in conventional freeze−thaw cycles, expected to address these challenges effectively through post-cross-linking during the gradual thawing phase.

To fabricate sponge materials with microscale pores using the freeze−thaw method, it is essential to control phase separation between polymers and ice crystals. Conventionally, the freeze−thaw method has been exploited for the preparation of hydrogels based on poly(vinyl alcohol), which

Received: May 6, 2024
Revised: July 4, 2024
Accepted: July 22, 2024
Published: August 16, 2024

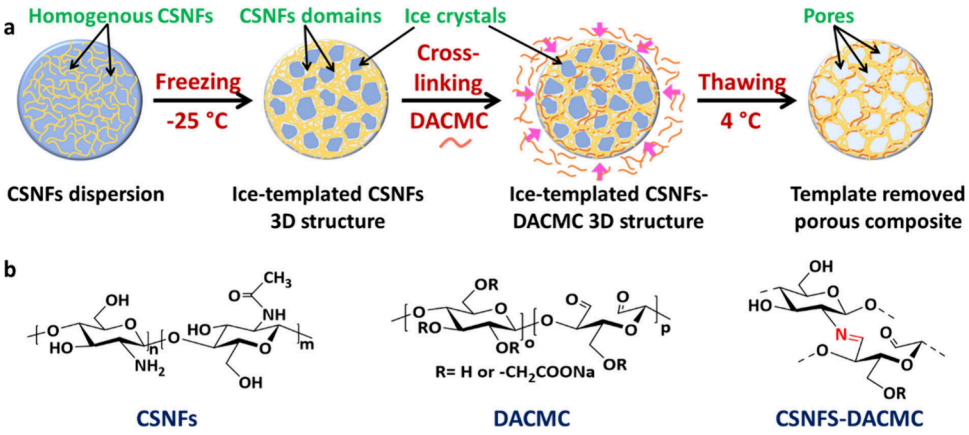

Figure 1. (a) Schematic of the CSNFs-DACMC composite fabrication using the freeze−thaw method. (b) Chemical structures of CSNFs and DACMC, highlighting the imine bonding.

is the most representative material, and polysaccharides including chitosan.[10−12] Most of these hydrogels exhibit transparent or translucent appearance and retain water in materials even when subjected to deformation, unlike sponge materials. These characters are derived from dense networks composed of well-hydrated polymers, sometimes resulting in negative performance derived from low diffusion and mass transfer capacity. In contrast, sponge materials can be created by the freeze−thaw process utilizing an aqueous suspension of fibers, instead of an aqueous solution of polymers. Freezing water in the presence of dispersed solid fiber leads to separation into the fiber-rich phase as matrix backbones and the large microscale ice crystal phase as pores. A stable porous network can be produced by the concentration of fibers, which leads to physical entanglement and interactions, and post-cross-linking. In the sponge materials, water is squeezed out by compression of the materials because the matrices derived from fibers are inherently not soluble in water even if hydrated to some extent. Furthermore, such sponge materials are expected to exhibit high water absorption and high mass diffusion capacity due to phase-separated solid matrices with large porosity.

Recently, there has been a significant increase in the use of biodegradable polymers as primary matrices, driven by escalating concerns over the depletion of fossil fuel resources and environmental challenges, including global warming.[13,14] Biomass wastes are particularly appealing in this context due to their recyclability, environmental sustainability, and cost-effectiveness, positioning them as superior candidates for such applications. Chitosan (CS), derived from an abundant supply of crustaceans and fungi, is a standout material. CS is the deacetylated derivative of chitin, which is the second most abundant natural polymer.[15,16] It is distinguished by its biocompatibility, nontoxicity, and biodegradability, which are inherent to polysaccharides. Additionally, CS is uniquely separable from other polysaccharides like cellulose and chitin due to its cationic nature and solubility in acidic aqueous solutions, facilitated by the presence of primary amino groups.[17,18] Chitosan nanofibers (CSNFs) have recently gained considerable interest as renewable building blocks for the development of functional materials. Various methods exist for fabricating CSNFs, including electrospinning, ultrasonication, grinding, atomization, and aqueous counter-collision (ACC). Notably, CSNFs produced using the ACC method with a high-pressure water jet system demonstrate exceptional features, such as fine micro- and nanoscale fibrous structures with extensive specific surface areas and stable high water dispersibility. Additionally, CSNFs exhibit superior physical properties due to the retention of CS's inherent structural integrity post-ACC treatment.[19] For the fabrication of sponge materials utilizing CS as a base material, employing CSNFs is advantageous because the nanofibers are initially separated from the aqueous media in the solid state. This biphasic condition of the nanofibrous suspension facilitates the formation of porous structures during the freeze−thaw process through a simple phase transition from the aqueous liquid phase to solid ice crystals acting as porogens. This leads to the formation of a CSNF-rich phase that forms the structural backbone of the porous material.[20] Consequently, CSNF-based sponges are expected to inherit beneficial properties such as a large specific surface area, high porosity, small pore size, and effective channel connectivity.[21]

The demand for fire retardancy (FR) and thermal insulation in polymer design, particularly in sectors such as construction, transportation, and aerospace, has increased significantly.[22,23] While CS-based materials are well-recognized for their biomedical applications, they are also being developed for flame-retardant and thermally insulated formulations that minimize environmental impact. Despite CS's intrinsic lack of FR properties, it has been demonstrated that combining CS with other polymers and/or flame-retardant additives enhances the FR behavior of the resultant materials significantly.[24,25] The FR properties are primarily derived from the role of CS as an exceptional carbon source that acts as an effective char-forming material, aiding in the suppression of flame spread. Moreover, the abundant amino groups in CS lend themselves to chemical modifications, such as incorporating phosphorus-based flame retardants and cross-linking, which mechanically stabilize the materials. Therefore, the development of CS-based sponge materials with robust FR properties is crucial for advancing toward a sustainable society, offering a preferable alternative to other nonbiobased and nonbiodegradable flame-retardant porous materials made from organic and inorganic substances.[26−29]

In this study, we introduce a method combining freeze−thaw and post-cross-linking techniques to develop stable CSNF-based sponge materials (see Figure 1). We employed CSNFs fibrillated using ACC as the matrix and dialdehyde carboxymethyl cellulose (DACMC), an oxidized derivative of carboxymethyl cellulose (CMC), as a cross-linking agent.[30]

https://doi.org/10.1021/acsomega.4c04317
ACS Omega 2024, 9, 36464−36474

During the freezing steps of the CSNFs aqueous suspension, ice crystals acted as a template for pore generation, inducing phase separation and the formation of a CSNF-rich phase. To enhance the physicochemical stability of the porous sponge structure, a cross-linking reaction was conducted by immersing the frozen CSNFs medium in a DACMC solution during the thawing step. The gradual diffusion of DACMC into the thawed sections of the CSNFs media facilitated the preservation of the porous structure originally templated by ice through cross-linking via ionic interactions and imine bonds, formed between the amino groups of CSNFs and the carboxyl and aldehyde groups of DACMC, respectively. This approach also resolves the challenge of polyion complex formation encountered when simply mixing cationic CSNFs with anionic DACMC, which impedes the creation of structured porosity through straightforward mixing. The optimal fabrication conditions for the sponge materials were investigated with regard to their mechanical strength, shape recoverability in the wet state and the morphology of the porous structures. Additionally, these materials have been employed for the adsorption of cationic and anionic dyes and metal ions. The FR properties under open flame conditions and thermal insulation properties under varying thermal states were also assessed and benchmarked against those of commercially available sponge materials. Given that the synthesis process avoids the use of toxic chemicals and relies on a straightforward methodology using natural-based polymers, this research contributes significantly to the development of eco-friendly approaches for producing multifunctional sponge materials.

EXPERIMENTAL DETAILS

Materials. CMC (0.65−0.90 carboxymethyl groups per anhydroglucose unit, approximately 9.0×10^4 g/mol average molecular weight) was obtained from Sigma-Aldrich (United States), CSNFs (derived from crab shell) from Sugino Machine Limited (Japan), and hydroxylamine hydrochloride (HAHCl) from Tokyo Chemical Industry Co., Ltd., Japan. Sodium periodate ($NaIO_4$), sodium hydroxide (NaOH), hydrochloric acid (HCl), Congo red (CR), methylene blue (MB), methyl orange (MO), and copper(II) chloride ($CuCl_2$) were sourced from FUJIFILM Wako Pure Chemical Corporation (Japan). All chemicals were used as received.

1. Preparation and Optimization of the CSNFs-DACMC Composite. Initially, an aqueous suspension of CSNFs was prepared. Acetic acid was added dropwise to the suspension, which was then stirred continuously overnight. The pH was adjusted to approximately 6.3 using this procedure. The concentration of CSNFs was varied at 1%, 1.5%, 2%, 2.5%, and 3 wt % to determine the optimal concentration. Subsequently, 2 mL of each concentration were dispensed into small glass vials and subjected to freezing at temperatures of −40 °C, −25 °C, and −10 °C. These samples were maintained at these temperatures for 12 h. An excess of DACMC solution in PBS buffer (5.0 wt %, pH 7.4) was then introduced to the samples (details of CMC oxidation and characterization are available in the Supporting Information). Following the addition of DACMC, thawing cycles were initiated, with samples maintained at 4 °C, 10 °C, and 25 °C for 12 h per cycle. This freeze−thaw process was repeated five times. Initially, 2 mL of DACMC solution was added to the frozen CSNFs suspension before the first thawing step. After completing the thawing step, the next freezing cycle was started with the whole mixture containing both CSNFs and DACMC. At the end of the thawing step of the third cycle, the supernatant was removed and another 2 mL of DACMC was added. After finishing the fifth cycle, the samples were rinsed with deionized water to remove any unreacted DACMC and were termed CSNF-DACMC composites. For drying, samples were frozen in liquid nitrogen and then lyophilized.

2. Characterization of the Samples. Material characterization was performed using attenuated total reflection-Fourier transform infrared (ATR-FTIR) spectroscopy (Thermo Scientific Nicolet iS5 equipped with an iD5 ATR attachment, United States), with scans conducted over a wavenumber range from 4000 to 500 cm^{-1}. The samples were frozen using liquid nitrogen and lyophilized in a vacuum freeze drier. The micromorphologies of the samples were examined using scanning electron microscopy (SEM) (Hitachi SU3500, Japan). For SEM analysis, lyophilized samples were coated with gold−palladium using an MSP-1S magnetron sputter (Vacuum Device Inc., Japan) and observed in high-vacuum mode at an acceleration voltage of 1.50 kV. Elemental analysis was carried out to determine the percentage content of carbon, hydrogen, and nitrogen in the CSNFs-DACMC composite sample collected at the inner part and the outer part. The carbon-based CSNFs: DACMC ratio was calculated related to the N content of the CSNFs control sample. The analyses were measured using JM 10 (J-Science Lab Co., Ltd., Japan).

The bulk density (d), water adsorption capacity, and porosity of the samples were analyzed using eqs 1, 2, and 3, respectively:

$$d = \frac{W_d}{v} \tag{1}$$

where W_d is the dry weight and v is the volume, which was calculated by considering the material as a cylinder.

$$\textit{Water adsorption capacity} = \frac{W_w - W_d}{W_d} 100 \tag{2}$$

where W_w is the wet weight obtained by simply removing the surface water, and W_d is the dry weight.

Porosity was evaluated using a method previously reported in the literature.[31] Initially, the volume (V) of the cylindrical sponge was determined. The initial dry weight (W_0) of each sample was recorded. Subsequently, the samples were immersed in 99 wt % ethanol at a temperature of 25 °C for 24 h. After immersion, the final weight (W_1) of each sample was measured. The density of ethanol (ρ) was also considered in these calculations.

$$\textit{Porosity} = \frac{W_1 - W_0}{\rho V} 100 \tag{3}$$

3. Mechanical Strength of the Samples. The mechanical strength of both dry and wet samples was assessed separately. For wet samples, measurement was performed with the samples immersed in deionized water at room temperature. A 50 N load cell was employed, and compression tests were conducted at a rate of 3.0 mm min^{-1} using a universal testing machine (UTM) (Shimadzu EZ Graph, Japan). Cyclic compression tests for wet samples involved varying the strain to 20%, 40%, 60%, and 80%. The durability of these samples was determined based on the stress values at 80% strain during 20 compression cycles.

https://doi.org/10.1021/acsomega.4c04317
ACS Omega 2024, 9, 36464−36474

For completely dried samples, linear compression was performed at a rate of 3 mm min^{-1} using a 500 N load cell. The Young's modulus of the samples was calculated within 10% of the strain in the stress−strain curve.

4. Determination of Thermal Insulation and Fire Retardancy. A composite sample fabricated under specific conditions—frozen temperature of −25 °C, thawing temperature of 4 °C, 2.5 wt % CSNFs concentration, and 5 wt % DACMC concentration—was utilized to evaluate thermal insulation and fire retardancy properties. Initially, thermal insulation properties were assessed using infrared thermography (FLIR, Sweden). A setup involving a hot plate maintained at 100 °C and a cool plate at −6 °C was established, with the dried CSNFs-DACMC composite placed between them, covered by a thin glass slide. Infrared (IR)images were captured at 1 min intervals for 30 min and subsequently at 10 min intervals for an additional hour to monitor the temperature on the material's surface. This behavior was benchmarked against commercially available sponges made from cellulose, polyurethane (PU), and polystyrene (PS).

Three types of standard evaluation were performed to investigate the flammability of the CSNFs-DACMC.

A combustion test was performed based on the UL94 HB flammability standard method. Three flat-rod-shaped specimens with 125 × 13 × 5 mm in their size were prepared. The samples were conditioned at 23 °C, RH 50% for 48 h before being subjected to combustion testing.

The limiting oxygen index (LOI) of the material was determined based on the method standardized by the Cabinet Order for Enforcement of the Fire Service Act ("Handling of "Flammability" and Test Methods for Nonflammability and Flame Retardancy of Synthetic Resins", Fire Service Act, Hazardous Materials, No. 50, Appendix 1, Japan). The measurement was performed by using an oxygen index measuring machine (Candle combustion tester, DC type, Toyo Seiki Seisaku-sho, Ltd., Japan). The samples were conditioned at 20 °C, RH 65% for 24 h before being subjected to the measurement.

Microscale combustion calorimetry (MCC) measurement was carried out based on ASTM D7309 (methods A and B) by using MCC-3X-UL (Govmark Ltd. (Deatak), United States). Approx.5 mg of samples was heated from 75 to 850 °C at a heating rate of 1.0 °C/sec in a stream of nitrogen (80 cm^3/min) and oxygen (20 cm^3/min). The measurements were performed at least three times to take average values.

5. Determination of Stability in Different pH Conditions. For mechanical strength assessment under varying pH conditions, a series of pH solutions (2, 4, 6, 7, 8, and 10) was prepared using 0.01 M HCl and NaOH. Samples fabricated under the stated conditions were immersed in these solutions for 1 week, after which mechanical strength measurements were taken. Additionally, swelling ratio and weight loss were determined. A control sample consisting only of CSNFs was prepared by freezing at −25 °C and subsequently drying using a freeze-dryer.

6. Evaluation of Dye Adsorption Behavior. To evaluate adsorption properties, aqueous solutions of CR, MB, and MO were prepared at a concentration of 10 mg/L. The composite samples were immersed in these solutions and agitated at 25 °C for 24 h. Post-treatment, the UV absorbance of the solutions was measured at 498 nm for CR, 664 nm for MB, and 464 nm for MO. The amount of dye adsorbed by the samples was quantified using calibration curves.

RESULTS AND DISCUSSION

The CSNF-DACMC composite sponge materials were developed using an integrated freeze−thaw method and a cross-linking reaction during the thawing stages. The design and fabrication strategy of the sponge materials are depicted in Figure 1a. The composite utilizes sustainable polysaccharides, with CSNFs serving as the primary structural component and DACMC functioning as the cross-linker. The CSNFs, commercially produced through ACC methods, demonstrated a high aspect ratio, with lengths in the hundreds of micrometers and a diameter of approximately 160 nm (Figure S1). DACMC, synthesized via the oxidation of CMC, acted as an effective cross-linking agent due to its carboxyl and aldehyde groups, which facilitated the formation of ionic interactions and imine bonds with the amino groups of CSNFs (Figure 1b).

The fabrication process began with the freezing of an aqueous CSNF dispersion. This freeze−thaw cycle promoted template growth, where ice crystals served as a template for the porous network (Figure 1a). The freezing of the aqueous suspension led to the formation of concentrated CSNF domains adjacent to the ice crystals.[32] Subsequently, the frozen CSNF medium was immersed in a DACMC aqueous solution at a carefully controlled thawing temperature. As the ice melted gradually during the thawing stage, DACMC was integrated into the 3D structure of the CSNF domains, reinforce the material through cross-linking between CSNFs and DACMC via ionic interactions and imine bonds. The diffusion of DACMC from the surface of the melting ice allowed for the maintenance of the 3D structure and shape of the materials, ensuring structural integrity even after the ice template had melted away. Repeated freeze−thaw cycles further solidified the stability of physical interactions, including ionic interactions between amino and carboxyl groups and hydrogen bonds, thanks to the abundance of hydroxyl (OH) groups in both CSNFs and DACMC. This method effectively created a robust, porous structure suitable for a variety of applications.

The CSNF-DACMC wet sponge materials were successfully fabricated after undergoing five freeze−thaw cycles, as depicted in Figure 2a and S2. These composites demonstrated exceptional shape recoverability in their wet state, able to return to their original form upon the release of compressive stress, as shown in Figure 2c. This resilience was evident during compression tests conducted in both axial and parallel

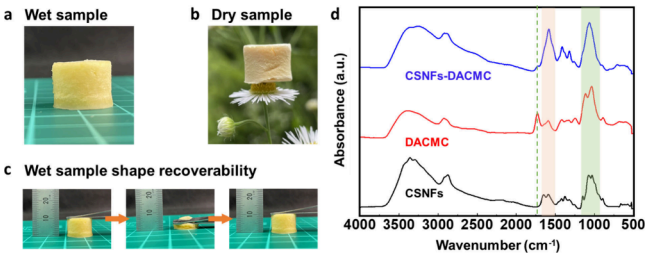

Figure 2. Photographs of the CSNFs-DACMC composite in (a) wet and (b) dry states. (c) Demonstrating the shape recoverability of the wet sample. (d) FTIR spectra for CSNFs, DACMC, and the CSNFs-DACMC composite.

https://doi.org/10.1021/acsomega.4c04317
ACS Omega 2024, 9, 36464−36474

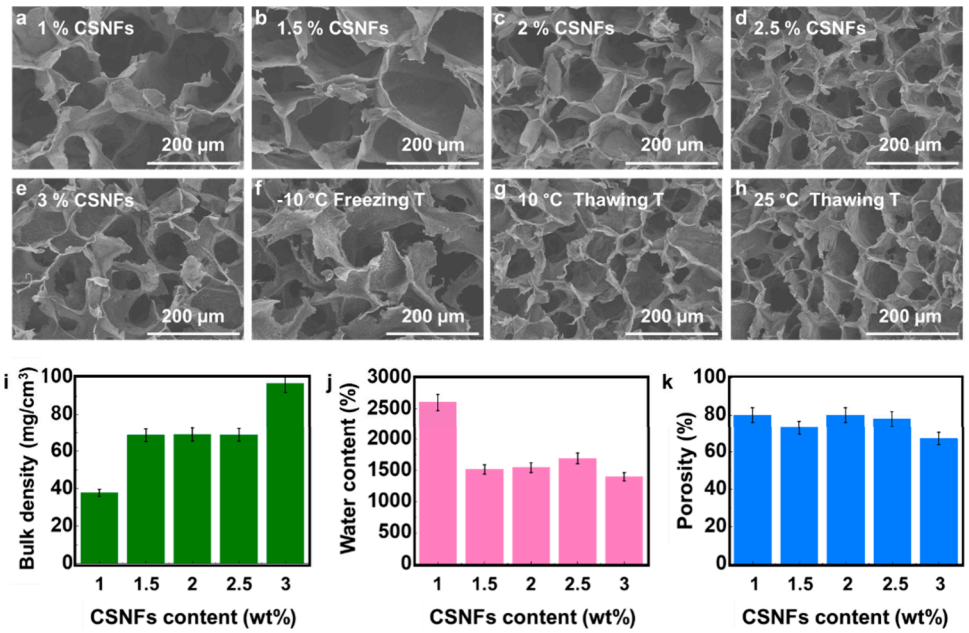

Figure 3. SEM images of CSNFs-DACMC composites with varying CSNF concentrations (1%, 1.5%, 2%, 2.5%, and 3%), frozen at −25 °C and thawed at 4 °C shown in (a−e). SEM image of the composite with 2.5 wt % CSNFs frozen at (f) −10 °C and (g) −25 °C and thawed at 10 °C and (h) 25 °C. Plots depicting (i) bulk density, (j) water content, and (k) porosity of the composites as functions of CSNF concentration.

directions, confirming the homogeneity and stability of the network (Supporting video 1a, 1b). Subsequently, the wet sponges were lyophilized to obtain dried porous materials, which displayed a remarkably low bulk density. The structural integrity was such that even thin flowers and stems could support the weight of the material, as illustrated in Figure 2b.

Fourier transform infrared (FTIR) spectroscopy was performed to characterize the chemical bonding within the materials (Figure 2d). For DACMC, a peak at 1590 cm^{-1} corresponding to the C═O stretching vibration of the carboxylate group was also observed in CMC (Figure S3). Additionally, a distinct peak at 1730 cm^{-1} in DACMC was identified as the C═O stretching vibration of the aldehyde group, indicative of the successful oxidation reaction facilitated by $NaIO_4$. The modification ratio of the aldehyde group was determined to be 6.5 ± 0.1 mmol/g through titration using hydroxylamine/NaOH (Scheme S2). In CS, the peak at 1500 cm^{-1} was associated with the N−H bending vibration of the amide group, and another at 1600 cm^{-1} with the C═O stretching of the amide group. Notably, in the CSNF-DACMC composites, the prominent aldehyde peak of DACMC at 1730 cm^{-1} was decreased, suggesting the formation of imine bonds. The peak around 1630 cm^{-1}, associated with the imine bond, was anticipated to appear. However, due to overlapping peaks in this region, a broad peak appeared within the range of 1580−1680 cm^{-1}. This observation corroborates the cross-linking via imine bonds between the aldehyde groups in DACMC and the amino groups in CSNFs within the composite materials, enhancing their structural and functional properties.

Elemental analysis was conducted to determine the DACMC content in the composite (Table S2). According to the calculations based on carbon/nitrogen ratios, the carbon-based ratio of CSNFs to DACMC was 100:58 in the inner part and 100:62 in the outer part of the material. These results indicate that the content of incorporated DACMC is nearly identical, 1:0.6, in both the inner and outer parts, supporting a homogeneous composition throughout the material.

In a control experiment to evaluate the effect of composite formation, a sample consisting solely of CSNFs (CSNFs foam) was prepared. This sample was fabricated by freezing the CSNFs aqueous media and omitting the DACMC solution during the thawing step, resulting in materials that failed to retain their shape. Consequently, these samples were prepared through freezing followed directly by lyophilization, bypassing the thawing process. Unlike the CSNF-DACMC composite, the CSNFs foam exhibited no shape recovery behavior in water and was completely deformed after compression (Figure S4). Additionally, a sample comprised only of DACMC (DACMC foam) was prepared by freezing and lyophilizing the DACMC aqueous solution. This sample disintegrated in water shortly after immersion. These observations underscore the crucial role of DACMC in enhancing the stability of the composite through cross-linking with CSNFs, and highlight the importance of the cross-linked 3D structure for the functional behavior of the sponge.

The internal morphologies of the samples were examined using SEM. The composite showcased a honeycomb-like porous structure, attributed to the random freezing of water and the aggregation of CSNFs. Importantly, the porous structure of the CSNF-DACMC composite was comparable to that of the CSNFs foam, indicating that the porous morphology was primarily established during the freezing process of the CSNFs media (Figure S5). The pore size varied depending on the synthesis conditions. Specifically, the pore size decreased from approximately 130 to 70 μm when the CSNF concentration was increased from 1.0 to 3.0 wt % (Figure 3a−e). This variation in pore size is mainly due to the change in ice crystal size during the freezing step; higher concentrations of CSNFs resulted in smaller ice crystals, as the presence of a larger number of fibrous polymer domains led to a separation into ice-rich and polymer-rich phases. Furthermore, the mobility of the fibers within the media was restricted

https://doi.org/10.1021/acsomega.4c04317
ACS Omega 2024, 9, 36464−36474

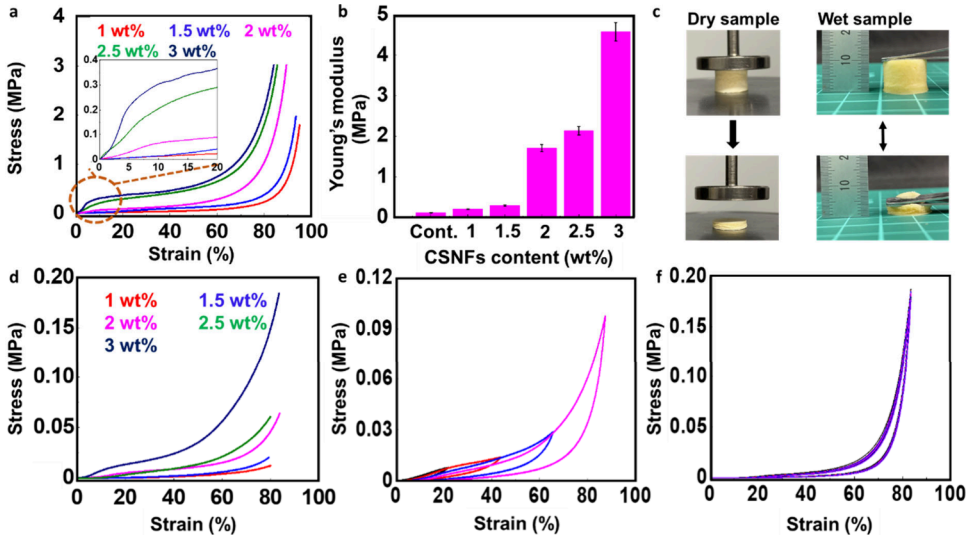

Figure 4. (a) Compression stress−strain curves for the dry CSNFs-DACMC composite. (b) Young's modulus of the dry composite across various CSNF concentrations. (c) Images showcasing shape recoverability comparing dry and wet states. (d) Compression stress−strain curves for the wet composite. (e, f) Cyclic compression stress−strain curves for the wet composite under different and constant strains, respectively, using samples with 2.5 wt % CSNFs frozen at −25 °C and thawed at 4 °C.

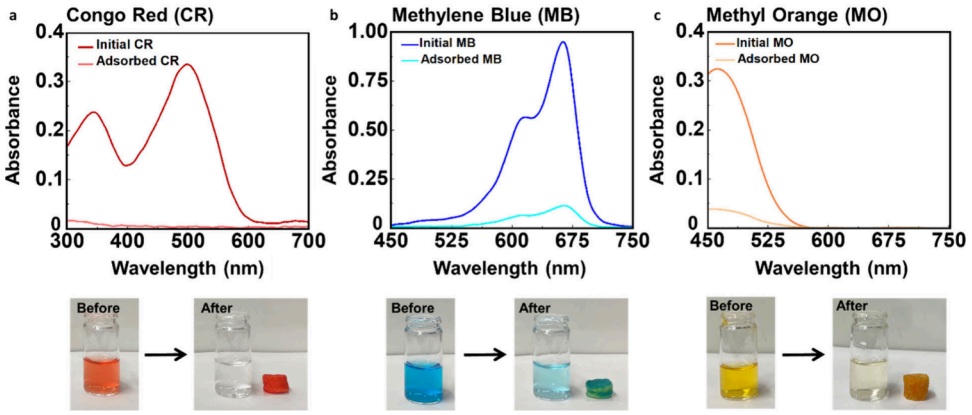

Figure 5. UV spectra and photographs of dye solutions (a) CR, (b) MB, and (c) MO before and after adsorption by the CSNFs-DACMC composite (2.5 wt %, FT −25 °C, TT 4 °C).

at higher viscosities and CSNF concentrations, resulting in the formation of smaller ice crystals. The walls of the skeletal backbone displayed a rougher and more fibrous morphology at higher CSNF concentrations, as depicted in Figure S6. Additionally, variations in freezing and thawing temperatures were explored. The pore size of the composite prepared at a freezing temperature of −10 °C was larger compared to that at −25 °C (Figure 3d, 3f). This difference is attributed to the fact that lower freezing temperatures result in faster freezing rates, thereby producing smaller ice crystals. These findings demonstrate that pore size can be adjusted by modifying the synthesis conditions. However, SEM images indicated that the thawing temperature did not significantly affect the pore size (Figure 3g, 3h).

The fundamental properties of the CSNF-DACMC sponge, such as density, water absorbency, and porosity, were thoroughly investigated. The density of the composite increased with CSNF concentration, with the sample containing 2.5 wt % CSNFs exhibiting a density of approximately 70 mg/cm^3 (Figure 3i). The densities of most samples remained below 100 mg/cm^3, classifying the sponge materials as low-density materials.[33] Water content, calculated based on the ratio of water to the dry weight of the composite, was approximately 1500%, except for the sample with 1.0 wt % CSNFs, which demonstrated outstanding water absorbency (Figure 3j). Moreover, nearly all samples exhibited more than 70% porosity (Figure 3k). From these results, it is evident that the CSNF-DACMC composite displays key characteristics of sponge materials, such as high porosity and excellent water absorbency, facilitated by its continuous honeycomb-like porous structure.

The mechanical properties of both wet and dry CSNF-DACMC composites were comprehensively evaluated. The dry samples displayed characteristics typical of an aerogel, which involved three distinct stages: initial low-strain linear elastic behavior, a yield area with a reduced slope, and a high-strain dense area. Notably, the mechanical properties such as Young's modulus were found to increase with the concentration of CSNFs (Figure 4a, 4b). The sample containing 3.0 wt % CSNFs, however, was brittle and fractured easily under compression. In contrast, the other samples could be compressed into thin discs without breaking (Figure 4c), and notably, these samples swelled back to their original cylindrical

https://doi.org/10.1021/acsomega.4c04317
ACS Omega 2024, 9, 36464−36474

shape upon immersion in water, demonstrating significant recoverability (Supporting video 2).

For the wet samples, mechanical strength also increased with CSNF concentration (Figure 4d). These samples exhibited repeated compressibility and the ability to recover to their initial state across all strain percentages (Figure 4e, 4f), which is characteristic of sponge materials. The mechanical strength notably increased with CSNF concentration (Figure S7). Samples with 2.5 and 2 wt % CSNFs exhibited smaller reductions in compression stress after successive cycles of compression and release compared to other samples. Optimal parameters were identified as 2.5 wt % CSNFs, a freezing temperature of −25 °C, and a thawing temperature of 4 °C, based on the observed energy dissipation behavior.

Additionally, the inherent primary amino groups of CS and the carboxylic groups of DACMC endow the materials with the capability to adsorb anionic and cationic materials.[15,34] CR was utilized to assess the adsorption behavior of CSNF-DACMC at a pH of 6.7. The material was able to adsorb approximately 98% of the dye from the solution (Figure 5a), with an adsorption capacity of 4.8×10^2 mg/g for CR. This high adsorption capacity primarily arises from the interactions between the cationic amino groups of the CSNFs and the sulfate anion of CR, illustrating the effectiveness of the composite in removing pollutants from aqueous solutions. Additionally, the amino group of CR can interact with the carboxylate anion of DACMC and possibly react with the residual aldehydes in DACMC. An adsorption experiment using cationic MB demonstrated that approximately 90% of MB was adsorbed at pH 10.2 (Figure 5b), with an adsorption capacity of 67 mg/g. The primary mechanism for the adsorption of cationic MB is attributed to electrostatic interactions with the anionic carboxylate anions of DACMC. In the case of the anionic dye MO, approximately 85% of the dye was adsorbed by the sample at pH 6.8, with an adsorption capacity of 56 mg/g (Figure 5c). Additionally, the composite material demonstrated the capability to adsorb Cu^{2+} ions, utilizing the chelation ability of CS, with an adsorption capacity of 75 mg/g (Figure S8).[35] These results underscore the composite's utility for adsorbing both anionic and cationic dyes as well as metal ions.

The FR properties of the CSNF-DACMC sponge materials were also evaluated. When exposed to an open flame, the CSNF-DACMC did not ignite (Supporting video 3a, 3b, 3c, and 3d). The material demonstrated self-extinguishing properties, as the flame did not propagate further and was extinguished immediately upon removal from the flame. This behavior contrasts starkly with that observed in commercially available cellulose, PS, and PU foams (Figure 6a, 6b, 6c, and 6d), which burned completely, leaving only ash. The FR properties, such as ignition time, flame transfer rate, and char formation rate, were further investigated (Table S1). While the edges of the cellulose, PS, and PU foams ignited rapidly, allowing the flame to spread quickly to the other side of the materials and resulting in complete combustion (Supporting video 4a, 4b, 4c, and 4d), the CSNF-DACMC sponge did not ignite and ceased burning upon removal from the flame, gradually forming a stable char layer. This resulted in a low char formation rate of 0.16 cm/s, as the formation of a protective char layer significantly hindered the spread of flames across the material's surface.

Following exposure to fire, the burned samples, including CSNFs foam, DACMC foam, and CSNF-DACMC composite sponges, were analyzed to assess the components contributing to their remarkable FR behavior. General fire retardancy mechanisms are typically categorized into two types. The first is intumescent FR behavior, where the material swells upon degradation and forms a porous foam structure, creating an effective barrier against heat, air, and pyrolysis products. The second mechanism involves char formation, where the material develops a dense and stable carbonaceous layer on its surface, blocking the diffusion of gaseous products to the flame and thereby shielding the underlying material from heat.[23] For the CSNFs foam, upon exposure to fire, it contracted and formed a char layer on the burned surface (Figure 7a). Despite the formation of dense structures within the char layers, a porous morphology was still discernible in the SEM images. The CSNFs displayed slight ignition, but the fire quickly extinguished, as captured in Supporting videos 5a and 5b. The DACMC foam primarily exhibited intumescent behavior. Figure 7b illustrates the swelling behavior of DACMC foam upon contact with the flame, resulting in an ash-like, fluffy, and unstable layer atop the sample. SEM images of the burned section revealed a slightly porous structure characteristic of intumescent fire retardancy. In contrast, the CSNF-DACMC composite sponge neither swelled significantly nor contracted dramatically upon exposure to flame but showed behavior akin to that of the CSNFs foam (Figure 7c). The char formed by the CSNF-DACMC sponge produced a continuous, layer-like structure that effectively covered and protected the lower parts of the sponge not directly in contact with the fire. Furthermore, when control samples of CSNF-DACMC films were subjected to an open flame, both film samples displayed slight ignition, with flame distribution observed in the Supporting videos 6a, 6b. These observations suggest that the integration of CSNFs and DACMC enhances the char formation and stability, contributing significantly to the fire-retardant properties of the composite material. The DACMC films demonstrated notable intumescent behavior upon exposure to fire, effectively swelling to form a protective layer. In the case of CSNF films, the spread of flame across the material was effectively suppressed due to the ability of CS to serve as an excellent carbon source for stable char layer

Figure 6. Photographs demonstrating the behavior under open flame of (a) CSNFs-DACMC (2.5 wt %, FT −25 °C, TT 4 °C) and commercial (b) cellulose, (c) PU, and (d) PS foams.

https://doi.org/10.1021/acsomega.4c04317
ACS Omega 2024, 9, 36464−36474

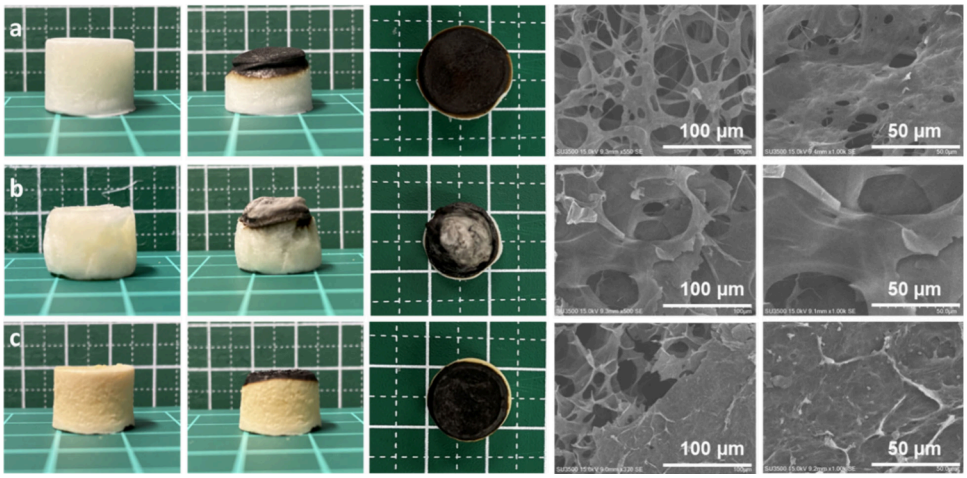

Figure 7. Photographs and SEM images of the char layer formation on (a) CSNFs, (b) DACMC foams, and (c) CSNFs-DACMC (2.5 wt %, FT −25 °C, TT 4 °C) after exposure to an open flame.

formation, thereby enhancing its FR properties.[25,36] Compared to individual films, the CSNF-DACMC composites exhibited enhanced FR properties, such as greater shape stability and a self-extinguishing nature. These results underscore that the CSNF-DACMC sponge materials display exceptional FR behavior due to their strong mechanical properties, which are derived from compositing with cross-linking and a porous morphology that facilitates the formation of a stable char layer.

The fire-retardant behavior was evaluated through standard flammability tests. First, the flammability of the CSNFs-DACMC was investigated based on the UL94 standard test. The level of the flame retardancy of the composite was UL94HB. As shown in Supporting video 7, during the combustion test, the sample did not ignite even after being exposed to the fire for 30 s. Flame never spread over the entire specimens and charring occurred only around the burned area.

Second, the limiting oxygen index (LOI) of the sample was evaluated (Table S3 and Figure S11). Table S3 presents the thermal combustion properties of the CSNFs-DACMC composite and several common polymers. The CSNFs-DACMC composite exhibited a higher LOI value of 36.4%, compared to cotton (18.4%)[37] and chitosan (27.6%).[38,39] The enhancement of LOI value was achieved by the combination of CSNFs and DACMC. The result suggests the stable cross-linked network among the polysaccharides enabled formation of dense char layer under combustion, contributing to excellent flame retardancy.

Finally, microscale combustion calorimetry (MCC) measurement was performed to further compare combustion behavior with common materials. The CSNFs-DACMC composite exhibited significantly low peak heat release rate (pHRR) and heat release capacity (η_c) (28 ± 0 W g^{-1} and 27.6 ± 0.3, J g^{-1} K^{-1}, respectively) compared to cotton (270 W $g^{-1}$and 235 J g^{-1} K^{-1}, respectively)[37] chitosan (102 J g^{-1} K^{-1})[39] and various common plastics (Figures 8 and S12 and Table S3). Remarkably, these values are also lower than those of halogenated polymers such as fluorinated ethylene propylene (FEP) (57 J g^{-1} K^{-1})[40] and poly(vinyl chloride) (PVC) (128 J g^{-1} K^{-1}),[40] supporting outstanding fire retardancy of the sponge material. Notably, the flame-retardant properties were achieved through the synergistic effect of combining CSNF and DACMC, without the addition of common flame-retardant additives such as phosphorus. In conclusion, the

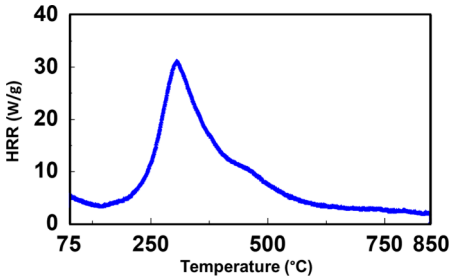

Figure 8. Heat release rate (HRR) curve of CSNFs-DACMC composites obtained from MCC test method A.

combination of chitosan and cellulose derivatives with stable cross-linked network structures will provide one strategy to create environmentally friendly fire-resistant materials.

Subsequently, the thermal insulation behavior of the CSNF-DACMC dry sponge was investigated. The sample was placed on a hot plate set at 100 °C and thermal behavior was monitored using an IR thermographic camera (Figure S9a). The temperatures of the heated sample surfaces and the glass plates positioned above them were individually recorded (Figure S9b). Similar examinations were conducted with cellulose, PS, and PU foams. The results revealed that the thermal insulation performance of the CSNF-DACMC composite surpassed that of the other commercial materials (Figure 9). The composite maintained a temperature of around 40 °C even after 1 h (Figure 9a, 9d). Additionally, when a glass plate was placed atop the sample, the temperature remained around 38 °C after 1 h (Figure 9b, 9e). When positioned on a cold plate, the temperature did not drop below 19 °C (Figure 9c, 9f), indicating robust thermal insulation in both hot and cold environments.

The composite's porous structure significantly contributes to this thermal insulation by impeding thermal convection. Furthermore, the 3D network acts as a thermal barrier by creating a complex path that hinders the transfer of heat waves. When the composite was placed on a hand and observed with an IR camera, it effectively blocked the thermal IR radiation emitted by the human body (Figure S9c). This characteristic suggests potential applications for the composite as an infrared camouflage material, utilizing its unique properties to enhance both safety and efficiency in various applications.

https://doi.org/10.1021/acsomega.4c04317
ACS Omega 2024, 9, 36464−36474

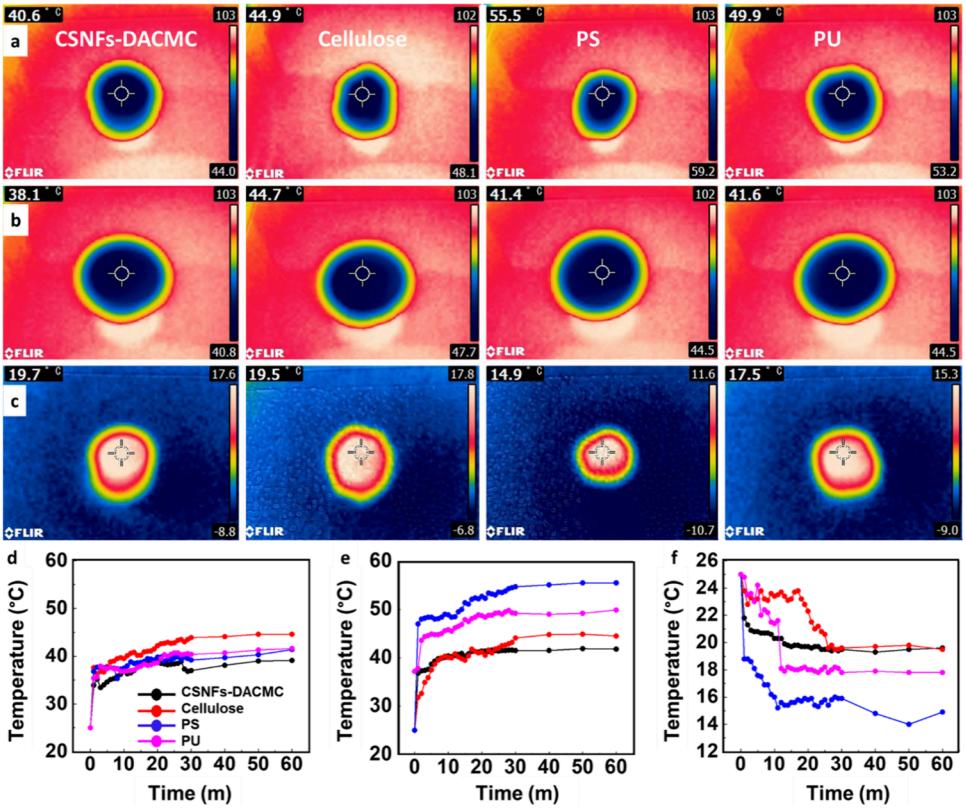

Figure 9. (a, d) IR images and time-to-temperature graphs for CSNFs-DACMC and commercial foams on a hot plate at 100 °C for 1 h. (b, e) IR images and time-to-temperature graphs for CSNFs-DACMC and commercial foams on a hot plate at 100 °C with a glass plate on top for 1 h. (c, f) IR images and time-to-temperature graphs for CSNFs-DACMC and commercial foams on a cold plate at −10 °C.

CS is recognized for its solubility in acidic solutions, a property attributed to the protonation of its primary amino groups under acidic conditions. While this characteristic can be advantageous, it poses challenges regarding the pH stability of CS-based materials for certain applications. To address these concerns, the stability of the CSNF-DACMC composite material under varying pH conditions was thoroughly evaluated. The optimized sponge was immersed in solutions with different pH values for 1 week, after which its mechanical strength was assessed. The stress−strain curves indicated that at a very low pH value of 2, the mechanical strength of the sponge decreased due to swelling in the highly acidic media. In contrast, at pH values of 4, 6, 7, and 8, the mechanical strength remained relatively unchanged; however, a slight increase in mechanical strength was observed at pH 10 (Figure S10a, b, and c). It was noted that all samples regained their original shapes after compression, with the exception of the sponge exposed to pH 2 (Figure S10e). Interestingly, while the material compressed into a thin disc at pH 2 did recover its original state upon the addition of water, this highlighted that the 3D structure was maintained despite deformation (Figure S10d). In a comparative analysis, the CSNFs foam, without the cross-linking and robust 3D structure of the composite, was unable to maintain its shape under the same acidic condition and disintegrated rapidly. These findings underscore the critical importance of a cross-linked 3D structure for maintaining the stability and functionality of CS-based sponges across a broad range of pH conditions. This structural integrity ensures that the composite materials can withstand various environmental stresses, making them suitable for diverse applications where pH fluctuations might otherwise compromise material performance.

CONCLUSIONS

Sponge materials comprising biomass resources, specifically CSNFs and DACMC, were successfully synthesized using a freeze−thaw method complemented by post-cross-linking during the thawing phase. This novel approach utilized ice crystals as a template for pore formation during the freezing steps of the CSNFs media, leading to the concentration of the CSNF-rich phase. Subsequent thawing facilitated the gradual diffusion of DACMC from the thawed CSNFs medium, enabling the formation of stable porous structures through ionic interactions and imine bonds. The resulting cross-linked structure enhanced the mechanical stability of the sponge and its overall porous integrity. The optimal parameters for fabrication were identified as 2.5 wt % CSNFs and 5 wt % DACMC, with a freezing temperature of −25 °C and a thawing temperature of 4 °C. These conditions yielded materials with superior properties. Under wet conditions, the material functioned effectively as a sponge, demonstrating exceptional shape recoverability. The CSNF-DACMC composite proved to be an effective adsorbent for both anionic and cationic dyes, utilizing the cationic nature of CS's amino groups and the anionic properties of DACMC's carboxylic acid groups. Additionally, the material exhibited the capacity to adsorb metal ions, such as Cu^{2+}, making it suitable for applications in wastewater purification due to the chelating ability of the amino groups in CSNFs. In its dry state, the CSNF-DACMC composite exhibited properties akin to those of an aerogel, serving as an excellent thermal insulator by

https://doi.org/10.1021/acsomega.4c04317
ACS Omega 2024, 9, 36464−36474

creating a complex pathway that impedes heat transfer in diverse thermal environments. Its insulation performance surpassed that of conventional commercial materials such as PS and PU foams. Moreover, the composite demonstrated outstanding fire-retardant properties by forming a stable char layer that effectively hindered combustion. The synthesis process, free from toxic chemicals and relying on natural-based polymers, represents a significant advancement in the development of eco-friendly methods for fabricating multifunctional materials. This study not only demonstrates the potential of CSNF-DACMC composites in various applications but also emphasizes the environmental benefits of using sustainable resources in material engineering.

■ ASSOCIATED CONTENT

Supporting Information

The Supporting Information is available free of charge at https://pubs.acs.org/doi/10.1021/acsomega.4c04317.

Movie S1a: shape recoverability of wet composite (MP4)

Movie S1b: shape recoverability of wet composite (MP4)

Movie S2: shape recoverability of dry composite by water adsorption (MP4)

Movie S3a: combustion of composite (MP4)

Movie S3b: combustion of commercial cellulose foam (MP4)

Movie S3c: combustion of commercial PU foam (MP4)

Movie S3d: combustion of commercial PS foam (MP4)

Movie S4a: char distribution of composite (MP4)

Movie S4b: char and flame distribution of commercial cellulose foam (MP4)

Movie S4c: char and flame distribution of commercial PU foam (MP4)

Movie S4d: char and flame distribution of commercial PS foam (MP4)

Movie S5a: combustion of composites (MP4)

Movie S5b: combustion of DACMC foam (MP4)

Movie S6a: combustion of CSNFs film (MP4)

Movie S6b: combustion of DACMC film (MP4)

Movie S7: UL94HB test (MP4)

Experimental process of CMC oxidation and aldehyde content determination in DACMC (Schemes S1, S2), SEM of CSNFs morphology (Figure S1), CSNFs-DACMC composite appearance in different FT cycles (Figure S2), FTIR spectra of CMC and DACMC (Figure S3), stability of water adsorbed control sample (CSNFs) and its inner morphology (Figures S4, S5), CSNFs-DACMC composite pore wall morphology change related to CSNF content (Figure S6), cyclic compression stress−strain curves of wet CSNFs-DACMC fabricated in different conditions (Figure 7), Cu^{2+} adsorption of composites (Figure S8), thermal insulation setup (Figure S9), properties of composite in different pH environments (Figure S10), maximum combustion rate of CSNFs-DACMC (Figure S11), HRR curve of composites (Figure S12), data of combustion tests (Table S1), elemental analysis (Table S2), thermal combustion properties (Table S3) (PDF)

■ AUTHOR INFORMATION

Corresponding Authors

Akihide Sugawara − *Department of Applied Chemistry, Graduate School of Engineering, Osaka University, Suita, Osaka 565-0871, Japan;* orcid.org/0000-0002-5060-0923; Email: a_sugawara@chem.eng.osaka-u.ac.jp

Hiroshi Uyama − *Department of Applied Chemistry, Graduate School of Engineering, Osaka University, Suita, Osaka 565-0871, Japan;* orcid.org/0000-0002-8587-2507; Email: uyama@chem.eng.osaka-u.ac.jp

Author

Madhurangika Panchabashini Horathal Pedige − *Department of Applied Chemistry, Graduate School of Engineering, Osaka University, Suita, Osaka 565-0871, Japan*

Complete contact information is available at: https://pubs.acs.org/10.1021/acsomega.4c04317

Notes

The authors declare no competing financial interest.

■ ACKNOWLEDGMENTS

This research was performed by the Environment Research and Technology Development Fund JPMEERF21S11900 of the Environmental Restoration and Conservation Agency of Japan and JSPS KAKENHI Grants (No. 22K20481, 23H02024), JST, CREST, Japan (Grant Number JPMJCR22L4), and Japan Science and Technology Agency (JST) Grant (No. JPMJPF2218). M.P.H.P. would like to thank the Ministry of Education, Culture, Sports, Science and Technology (MEXT) for scholarship support.

■ REFERENCES

(1) Kargarzadeh, H.; Huang, J.; Lin, N. Recent developments in nanocellulose-based biodegradable polymers, thermoplastic polymers, and porous nanocomposites. *Prog. Polym. Sci.* **2018**, *87*, 197.

(2) Usmani, A. M.; Salyer, I. O. Open Pore Polymer Structures: A Review. *Polym. Plast. Technol. Eng.* **1979**, *12*, 61.

(3) Shin, Y. E.; Sa, Y. J.; Park, S. An ice-templated, pH-tunable self-assembly route to hierarchically porous graphene nanoscroll networks. *Nanoscale* **2014**, *6*, 9734.

(4) Starbird, R.; García-González, C. A.; Smirnova, I.; Krautschneider, W. H.; Bauhofer, W. Synthesis of an organic conductive porous material using starch aerogels as template for chronic invasive electrodes. *Mater. Sci. Eng., C* **2014**, *37*, 177.

(5) Wang, Y.; Zhang, J.; Chen, S.; Zhang, X.; Li, Y.; Yang, Z. Vapor-Responsive Shape-Memory Material Based on Carbon Nanotube Sponge Dominated by Pressure-Induced Conformational Transition of Spidroin. *ACS Appl. Polym. Mater.* **2023**, *5*, 2490.

(6) Duan, G.; Jiang, S.; Moss, T.; Agarwal, S.; Greiner, A. Ultralight open cell polymer sponges with advanced properties by PPX CVD coating. *Polym. Chem.* **2016**, *7*, 2759.

(7) Takase, H.; Shiomori, K.; Okamoto, Y.; Watanabe, N.; Matsune, H.; Umakoshi, H. Micro Sponge Balls: Preparation and Characterization of Sponge-like Cryogel Particles of Poly(2-hydroxyethyl methacrylate) via the Inverse Leidenfrost Effect. *ACS Appl. Polym. Mater.* **2022**, *4*, 7081.

(8) Zhang, L.; Wang, Y.; Chang, C. Effects of freezing/thawing cycles and cellulose nanowhiskers on structure and properties of biocompatible starch/pva sponges. *Macromol. Mater. Eng.* **2010**, *295*, 137.

(9) Bernal-Chávez, S. A.; Romero-Montero, A.; Hernández-Parra, H. Enhancing chemical and physical stability of pharmaceuticals using freeze-thaw method: challenges and opportunities for process

optimization through quality by design approach. *J. Biol. Eng.* **2023**, *17*, 35.
(10) Sekine, Y.; Nankawa, T.; Yunoki, S.; Sugita, T.; Nakagawa, H.; Yamada, T. Eco-friendly Carboxymethyl Cellulose Nanofiber Hydrogels Prepared via Freeze Cross-Linking and Their Applications. *ACS Appl. Polym. Mater.* **2020**, *2*, 5482.
(11) Park, E.; Ryu, J. H.; Lee, D.; Lee, H. Freeze-Thawing-Induced Macroporous Catechol Hydrogels with Shape Recovery and Sponge-like Properties. *ACS Biomater. Sci. Eng.* **2021**, *7*, 4318.
(12) Figueroa-Pizano, M. D.; Vélaz, I.; Peñas, F. J. Effect of freeze-thawing conditions for preparation of chitosan-poly (vinyl alcohol) hydrogels and drug release studies. *Carbohydr. Polym.* **2018**, *195*, 476.
(13) Cheung, Y. H.; Ma, K.; Wasson, M. C. Environmentally Benign Biosynthesis of Hierarchical MOF/Bacterial Cellulose Composite Sponge for Nerve Agent Protection. *Angew. Chem. Int. Ed* **2022**, *61*, No. e202202207.
(14) Wang, G.; Liu, X.; Song, Z. Multifunctional Flexible Pressure Sensor Based on a Cellulose Fiber-Derived Hierarchical Carbon Aerogel. *ACS Appl. Electron Mater.* **2023**, *5*, 1581.
(15) Wang, M.; Ma, Y.; Sun, Y. Hierarchical Porous Chitosan Sponges as Robust and Recyclable Adsorbents for Anionic Dye Adsorption. *Sci. Rep.* **2017**, *7*, 18054.
(16) Li, L.; Yang, H.; Li, X. Natural silk nanofibrils as reinforcements for the preparation of chitosan-based bio nanocomposites. *Carbohydr. Polym.* **2021**, *253*, No. 117214.
(17) Sánchez-Machado, D. I., López-Cervantes, J, Correa-Murrieta, M. A., Sánchez-Duarte, R. G., Cruz-Flores, P, la Mora-López, G. S. Chitosan. In *Nonvitamin and Nonmineral Nutritional Supplements*; Sayed, M. N., Ana, S. S., Eds; Elsevier: CA, 2018; p 485.
(18) Takeshita, S.; Zhao, S.; Malfait, W. J.; Koebel, M. M. Chemistry of Chitosan Aerogels: Three-Dimensional Pore Control for Tailored Applications. *Angew. Chem. - International Edition* **2021**, *60*, 9828.
(19) Ogura, K.; Brasselet, C.; Cabrera-Barjas, G.; et al. Production of Fungal Nanochitosan Using High-Pressure Water Jet System for Biomedical Applications. *Materials* **2022**, *15*, 1375.
(20) Zong, D.; Zhang, X.; Yin, X.; et al. Electrospun Fibrous Sponges: Principle, Fabrication, and Applications. *Advanced Fiber Materials* **2022**, *4*, 1434.
(21) Risch, P.; Adlhart, C. A Chitosan Nanofiber Sponge for Oyster-Inspired Filtration of Microplastics. *ACS Appl. Polym. Mater.* **2021**, *3*, 4685.
(22) Liu, C.; Wu, S.; Yang, Z.; et al. Mechanically Robust and Flame-Retardant Silicon Aerogel Elastomers for Thermal Insulation and Efficient Solar Steam Generation. *ACS Omega.* **2020**, *5*, 8638.
(23) Liu, B. W.; Zhao, H. B.; Wang, Y. Z. Advanced Flame-Retardant Methods for Polymeric Materials. *Adv. Mater.* **2022**, *34*, No. 2107905.
(24) He, H.; Wang, Y.; Yu, Z.; Liu, J.; Zhao, Y.; Ke, Y. Ecofriendly flame-retardant composite aerogel derived from polysaccharide: Preparation, flammability, thermal kinetics, and mechanism. *Carbohydr. Polym.* **2021**, *269*, No. 118291.
(25) Malucelli, G. Flame-retardant systems based on chitosan and its derivatives: State of the art and perspectives. *Molecules* **2020**, *25*, 4046.
(26) Zhang, S.; Liu, X.; Jin, X.; Li, H.; Sun, J.; Gu, X. The novel application of chitosan: Effects of cross-linked chitosan on the fire performance of thermoplastic polyurethane. *Carbohydr. Polym.* **2018**, *189*, 313.
(27) Yu, H.; Xu, X.; Xia, Y.; et al. Synthesis of a novel modified chitosan as an intumescent flame retardant for epoxy resin. *e-Polym.* **2020**, *20*, 303.
(28) Makhlouf, G.; Abdelkhalik, A.; Ameen, H. Preparation of highly efficient chitosan-based flame retardant coatings with good anti-bacterial properties for cotton fabrics. *Prog. Org. Coat.* **2022**, *163*, No. 106627.
(29) Carosio, F.; Ghanadpour, M.; Alongi, J.; Wågberg, L. Layer-by-layer-assembled chitosan/phosphorylated cellulose nanofibrils as a bio-based and flame protecting nano-exoskeleton on PU foams. *Carbohydr. Polym.* **2018**, *202*, 479.
(30) Sethi, S.; Kaith, B. S.; Kaur, M.; Sharma, N.; Khullar, S. A hydrogel based on dialdehyde carboxymethyl cellulose−gelatin and its utilization as a bio adsorbent. *J. Chem. Sci.* **2020**, *132*, 15.
(31) Yang, X.; Yang, D.; Lin, X.; et al. Effect of Dehydrothermal Treatment on the Structure and Properties of a Collagen-Based Heterogeneous Bilayer Membrane. *ACS Appl. Polym. Mater.* **2023**, *5*, 3427.
(32) Zhang, M.; Jiang, S.; Han, F.; Li, M.; Wang, N.; Liu, L. Anisotropic cellulose nanofiber/chitosan aerogel with thermal management and oil absorption properties. *Carbohydr. Polym.* **2021**, *264*, No. 118033.
(33) Jiang, S.; Agarwal, S.; Greiner, A. Offenzellige Schwämme mit niedrigen Dichten als Funktionsmaterialien. *Angew. Chem.* **2017**, *129*, 15726.
(34) Mohamed, E. N.; Abd-Elhamid, A. I.; El-Bardan, A. A.; Soliman, H. M. A.; Mohy-Eldin, M. S. Development of carboxymethyl cellulose-graphene oxide biobased composite for the removal of methylene blue cationic dye model contaminate from wastewater. *Sci. Rep.* **2023**, *13*, 14265.
(35) Hajili, E.; Sugawara, A.; Asoh, T. A.; Uyama, H. Fabrication of 3D Hierarchically Porous Chitosan Monoliths by Thermally Induced Phase Separation of Chemically Modified Chitin. *ACS Sustain. Chem. Eng.* **2023**, *11*, 5473.
(36) Kundu, C. K.; Hossen, M. T.; Islam, T.; Mollick, S.; Song, L.; Hu, Y. Flame Retardant Coatings from Bio-Derived Chitosan, Sodium Alginate, and Metal Salts for Polyamide 66 Textiles. *ACS Omega* **2022**, *7*, 30841.
(37) Yang, C. Q.; He, Q.; Lyon, R. E.; Hu, Y. Investigation of the flammability of different textile fabrics using micro-scale combustion calorimetry. *Polym. Degrad. Stab.* **2010**, *95*, 108.
(38) Chen, J.; Huang, W.; Chen, Y.; et al. Facile Preparation of Chitosan-Based Composite Film with Good Mechanical Strength and Flame Retardancy. *Polymers (Basel)* **2022**, *14*, 1337.
(39) Thomas, A.; Moinuddin, K.; Zhu, H.; Joseph, P. Passive fire protection of wood using some bio-derived fire retardants. *Fire. Saf. J.* **2021**, *120*, No. 103074.
(40) Lyon, R. E., Walters, R. N., Stoliarov, S. I. Screening flame retardants for plastics using microscale combustion calorimetry. In *Polymer Engineering and Science*; John Wiley and Sons Inc, 2007; p 1501.

https://doi.org/10.1021/acsomega.4c04317
ACS Omega 2024, 9, 36464−36474